Supplementary Information

Glacier changes across Subantarctic Heard Island revealed by remote sensing and ice thickness inversions

Weilin Yang[1,2], Levan G. Tielidze[1,2,3], Regine Hock[4,5], Bethan J. Davies[6], Steven L. Chown[7], Duane D. McKenna[8], Sarah S. Thompson[9], Justine D. Shaw[10], Andrew N. Mackintosh[1,2]

[1]School of Earth, Atmosphere and Environment, Faculty of Science, Monash University, Clayton, Melbourne, VIC 3800, Australia
[2]Securing Antarctica's Environmental Future, School of Earth, Atmosphere and Environment, Monash University, Clayton, Melbourne, VIC 3800, Australia
[3]Glaciology Research Centre, School of Natural Sciences and Medicine, Ilia State University, Tbilisi 0179, Georgia
[4]Department of Geosciences, University of Oslo, Oslo 0316, Norway
[5]Geophysical Institute, University of Alaska, Fairbanks, Fairbanks, Alaska 99775-7320, USA
[6]School of Geography, Politics and Sociology, Newcastle University, Newcastle upon Tyne NE1 7RU, UK
[7]Securing Antarctica's Environmental Future, School of Biological Sciences, Monash University, Victoria, 3800, Australia
[8]Department of Biological Sciences, and Center for Biodiversity Research, University of Memphis, Memphis, TN 38152, USA
[9]Australian Antarctic Program Partnership, Institute for Marine and Antarctic Studies, University of Tasmania, Hobart, TAS 7001, Australia
[10]Securing Antarctica's Environmental Future, Australian Antarctic Division, Department of Climate Change, Energy, the Environment and Water, Kingston 7050, Tasmania, Australia

Correspondence to: Weilin Yang (weilinyang.yang@monash.edu and ywlcwc@gmail.com)

This document includes:

Supplementary Table 1

Supplementary Figs. 1 to 7

Supplementary References

Table S1. Characteristics of individual glaciers in the 2019 Heard Island glacier inventory (Tielidze et al., 2025). Glacier numbers follow the sequence assigned to the 2019 outlines shown in Fig. 1. Glacier centroid coordinates and areas were calculated separately for each 2019 outline. Where a glacier mapped in 1988 or 2001 had split into multiple smaller glaciers by 2019, the resulting 2019 outlines inherited the corresponding glacierwide mass balance. The exact DEM acquisition dates for mass balance calculation are provided in Fig. S1. Uncertainties are reported as $\pm 1\sigma$.

No.	Central latitude	Central longitude	Area in 2019 (km^2, $\pm 1\sigma$)	Specific mass balance from 2000 to 2019 (m w.e. yr^{-1}, $\pm 1\sigma$)	Volume in 2019 (km^3, $\pm 1\sigma$)
1	53° 4.2′ S	73° 34.7′ E	1.00 ± 0.05	-0.06 ± 0.02	0.07 ± 0.01
2	53° 4.6′ S	73° 35.1′ E	7.05 ± 0.19	-0.06 ± 0.02	0.55 ± 0.11
3	53° 5.0′ S	73° 35.9′ E	6.30 ± 0.18	-0.25 ± 0.02	0.51 ± 0.11
4	53° 5.2′ S	73° 37.3′ E	3.80 ± 0.11	-0.72 ± 0.05	0.29 ± 0.06
5	53° 6.2′ S	73° 36.7′ E	11.65 ± 0.24	-1.10 ± 0.08	0.90 ± 0.19
6	53° 7.2′ S	73° 37.1′ E	6.68 ± 0.16	-0.35 ± 0.03	0.56 ± 0.12
7	53° 8.0′ S	73° 36.1′ E	9.86 ± 0.26	-0.39 ± 0.03	0.65 ± 0.14
8	53° 9.3′ S	73° 33.6′ E	21.77 ± 0.34	-0.33 ± 0.03	1.97 ± 0.41
9	53° 10.0′ S	73° 31.3′ E	2.07 ± 0.10	-0.33 ± 0.05	0.09 ± 0.02
10	53° 9.6′ S	73° 30.4′ E	1.08 ± 0.07	-0.52 ± 0.10	0.04 ± 0.01
11	53° 8.0′ S	73° 30.3′ E	32.32 ± 0.30	-0.17 ± 0.01	3.19 ± 0.66
12	53° 7.7′ S	73° 27.6′ E	19.72 ± 0.20	-0.21 ± 0.02	1.66 ± 0.35
13	53° 6.2′ S	73° 26.7′ E	19.94 ± 0.23	-0.30 ± 0.03	1.66 ± 0.34
14	53° 4.9′ S	73° 26.2′ E	8.41 ± 0.18	-0.19 ± 0.02	0.78 ± 0.16
15	53° 4.1′ S	73° 25.2′ E	7.64 ± 0.15	-0.45 ± 0.05	0.84 ± 0.18
16	53° 3.3′ S	73° 26.9′ E	15.89 ± 0.22	-0.21 ± 0.02	1.45 ± 0.30
17	53° 2.5′ S	73° 28.0′ E	1.79 ± 0.07	-0.33 ± 0.04	0.09 ± 0.02
18	53° 3.1′ S	73° 29.2′ E	8.04 ± 0.17	-0.09 ± 0.02	0.63 ± 0.13
19	53° 2.5′ S	73° 30.2′ E	2.13 ± 0.08	-0.25 ± 0.04	0.10 ± 0.02
20	53° 2.9′ S	73° 31.4′ E	15.53 ± 0.27	-0.10 ± 0.02	1.67 ± 0.35
21	53° 3.4′ S	73° 33.3′ E	19.26 ± 0.27	-0.05 ± 0.01	1.90 ± 0.40
22	53° 4.0′ S	73° 34.3′ E	1.53 ± 0.07	-0.05 ± 0.01	0.11 ± 0.02
23	53° 0.8′ S	73° 20.8′ E	0.06 ± 0.01	-0.18 ± 0.11	0.00 ± 0.00
24	53° 0.7′ S	73° 20.5′ E	0.03 ± 0.01	0.28 ± 0.28	0.00 ± 0.00
25	53° 0.6′ S	73° 20.4′ E	0.00 ± 0.00	0.13 ± 0.10	0.00 ± 0.00
26	53° 0.7′ S	73° 20.2′ E	0.09 ± 0.02	-0.20 ± 0.12	0.00 ± 0.00
27	53° 0.7′ S	73° 19.9′ E	0.02 ± 0.01	-0.20 ± 0.12	0.00 ± 0.00
28	53° 0.6′ S	73° 19.8′ E	0.06 ± 0.02	0.13 ± 0.10	0.00 ± 0.00
29	53° 0.5′ S	73° 19.6′ E	0.06 ± 0.01	0.13 ± 0.10	0.00 ± 0.00
30	53° 0.1′ S	73° 19.0′ E	0.25 ± 0.03	-0.46 ± 0.14	0.00 ± 0.00
31	52° 59.7′ S	73° 19.2′ E	0.60 ± 0.05	-0.46 ± 0.14	0.02 ± 0.00
32	53° 0.0′ S	73° 17.9′ E	0.28 ± 0.02	-0.35 ± 0.22	0.01 ± 0.00
33	52° 59.9′ S	73° 17.3′ E	0.26 ± 0.03	-0.24 ± 0.12	0.00 ± 0.00
34	52° 59.7′ S	73° 17.4′ E	0.27 ± 0.03	-0.30 ± 0.10	0.01 ± 0.00
35	52° 59.7′ S	73° 17.8′ E	0.24 ± 0.02	0.00 ± 0.11	0.00 ± 0.00

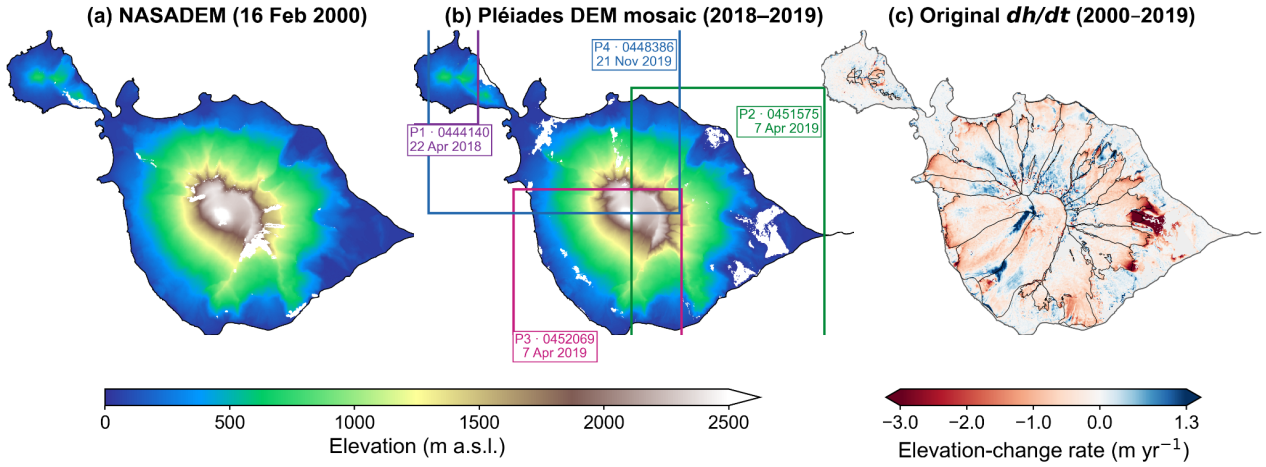

Figure S1. DEMs used to calculate the glacier mass balance of Heard Island: **(a)** NASADEM (NASA JPL, 2020) and **(b)** Pléiades DEM mosaic (Berthier et al., 2024). Coloured boxes in **(b)** indicate the coverage and acquisition dates of the four Pléiades DEMs. **(c)** Original elevation-change rate (*dh/dt*) derived from the co-registered NASADEM and Pléiades DEMs before gap filling. The colour bar range was capped at approximately the 99th percentile.

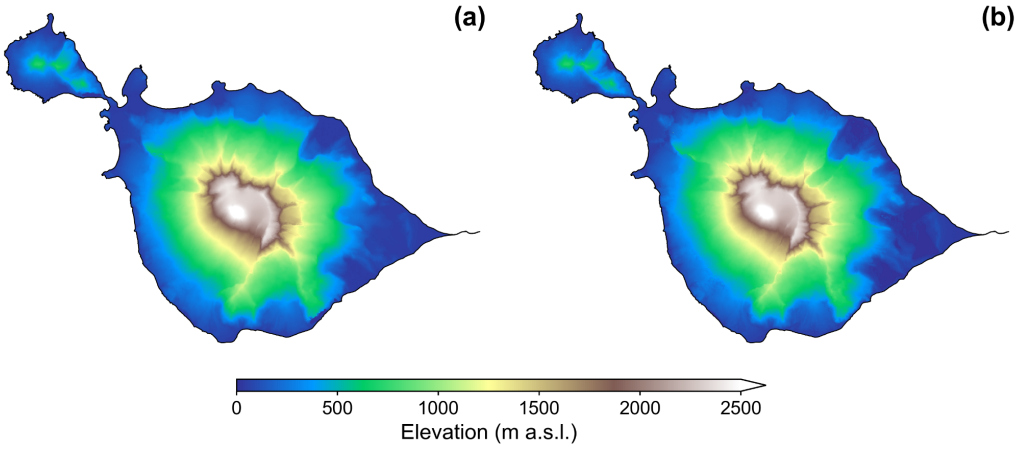

Figure S2. DEMs used for the glacier ice thickness inversions on Herad Island. **(a)** The 2000 NASADEM (NASA JPL, 2020), with local data gaps filled using ASTER GDEM V3 (NASA/METI/AIST/Japan Space systems and U.S./Japan ASTER Science Team., 2019). **(b)** The 2019 Pléiades DEM mosaic (Berthier et al., 2024), with local data gaps filled using the Copernicus DEM GLO-30 (European Space Agency, 2021). Both DEMs are shown at 20 m spatial resolution.

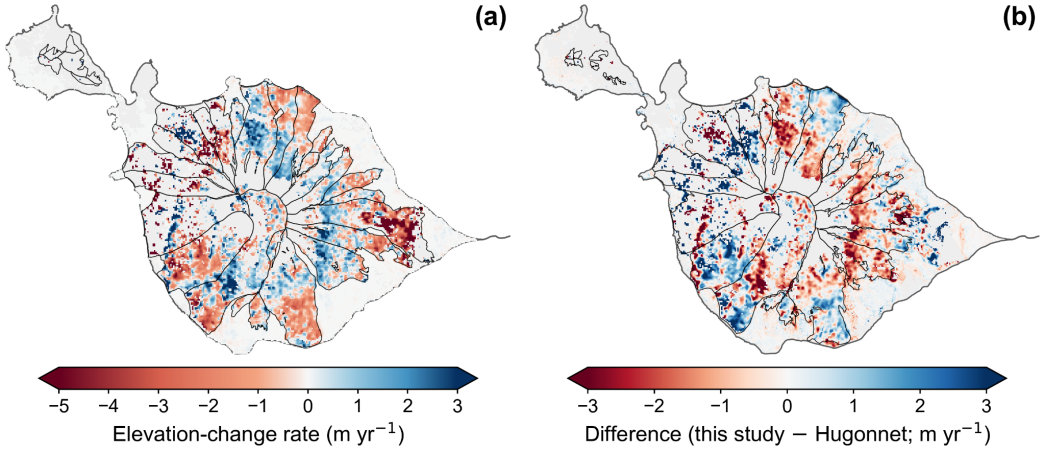

Figure S3. (a) *dh/dt* over Heard Island from Hugonnet et al., (2021) for the period from 1 January 2000 to 1 January 2020. **(b)** Differences between the original *dh/dt* obtained in this study (Fig. S1c) and those of Hugonnet et al., (2021). The 100 m Hugonnet et al. (2021) product was bilinearly resampled to the 20 m grid of this study before differencing, and only pixels valid in both datasets are shown. Black lines represent the RGI 6.0 glacier outlines (RGI Consortium, 2017) in panel **(a)** and the 2019 glacier outlines in panel **(b)**.

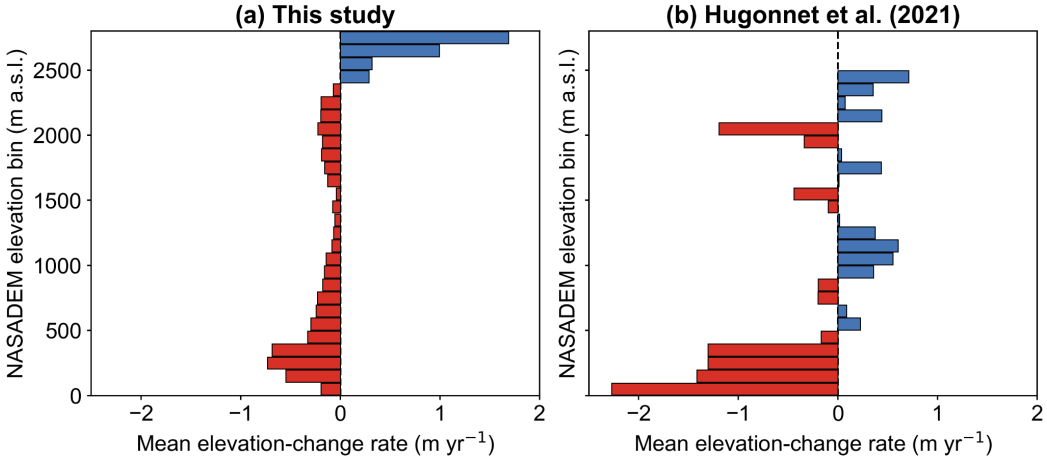

Figure S4. Mean *dh/dt* within 100 m NASADEM elevation bins for **(a)** this study and **(b)** Hugonnet et al. (2021). Red and blue bars represent negative and positive mean *dh/dt*, respectively. Elevation bins containing fewer than 5 valid *dh/dt* pixels were excluded.

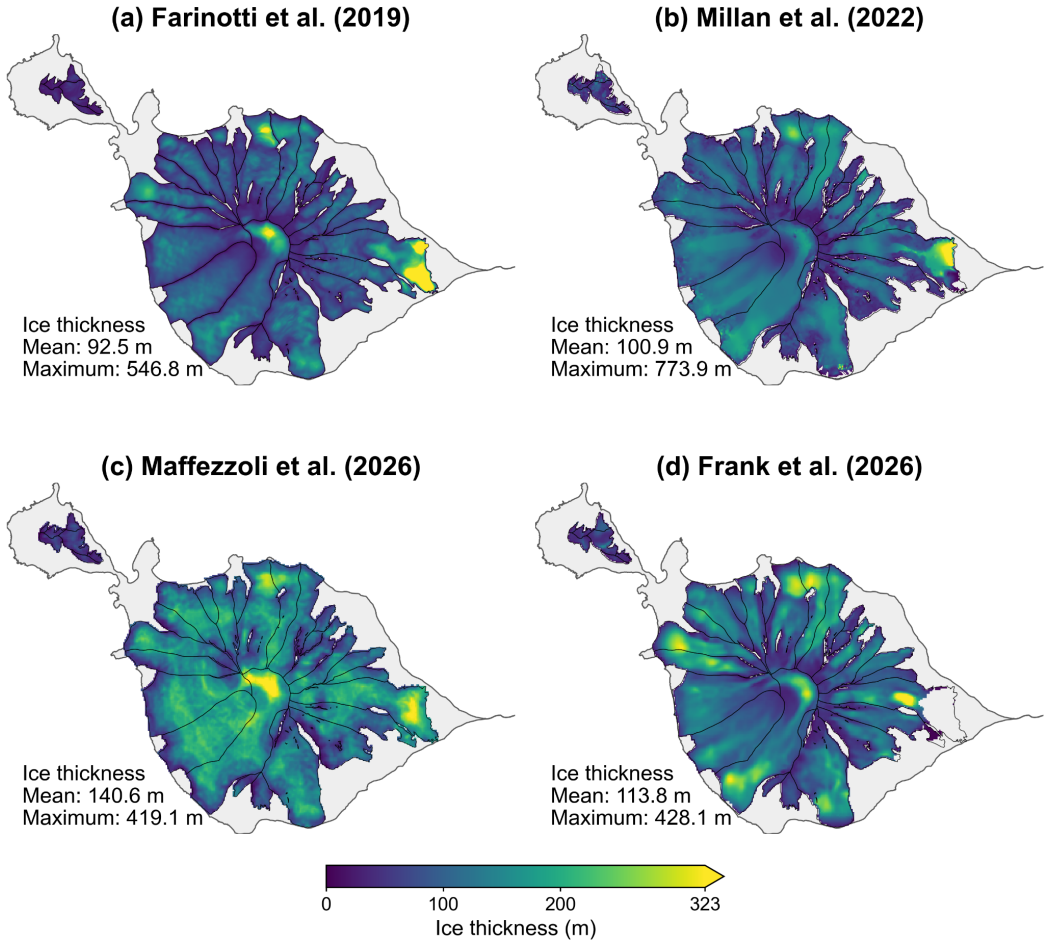

Figure S5. Spatial distributions of ice thickness across Heard Island from **(a)** Farinotti et al. (2019), **(b)** Millan et al. (2022), **(c)** Maffezzoli et al. (2026), and **(d)** Frank et al. (2026). Black lines indicate the glacier outlines used by each product: RGI 6.0 (RGI Consortium, 2017) in panels **(a)**, **(b)**, and **(d)**, and RGI 7.0 (RGI Consortium, 2023) in panel **(c)**. Both panels use the same colour scale as Fig. 5.

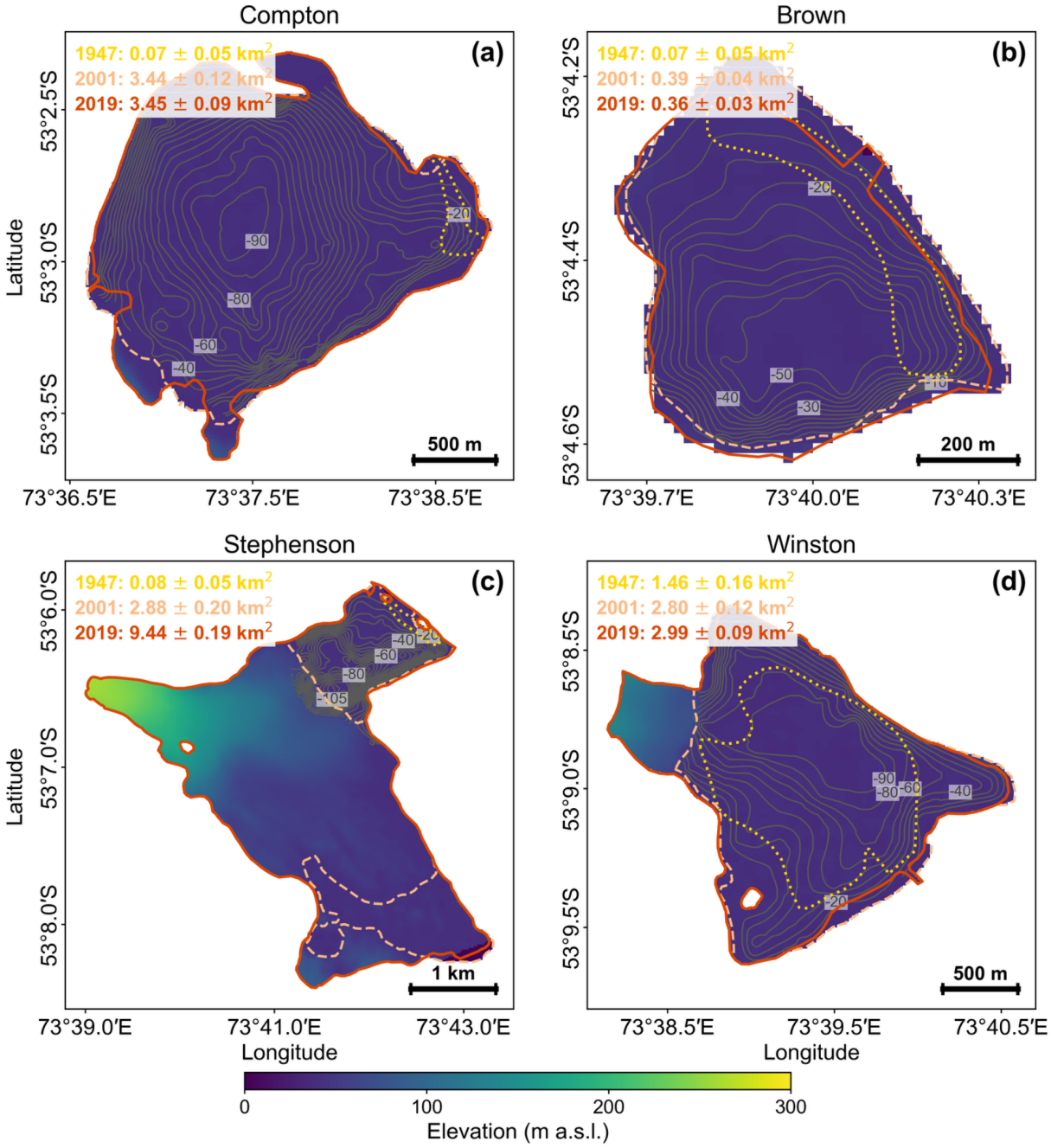

Figure S6. Lagoon outlines in 1947, 2001 and 2019 for **(a)** Compton, **(b)** Brown, **(c)** Stephenson, and **(d)** Winston Lagoons. The 1947, 2001, and 2019 lagoon extents were mapped from 1947 aerial imagery (Division of National Mapping, 1964), Landsat 7 ETM+ imagery (EROS Center, 2020) acquired on 31 January 2001, and 2018–2019 Pléiades imagery (Berthier et al., 2024), respectively. Lagoon boundaries along the glacier fronts were delineated following the glacier termini, while the remaining shorelines were mapped along the visible water margins. Mapping uncertainties were estimated using the same buffer approach described in Sect. 3.1. The 2004 lagoon bathymetry contours are from Donoghue (2009) and digitized by this study using QGIS v4.0.0. The background is 2000 NASADEM.

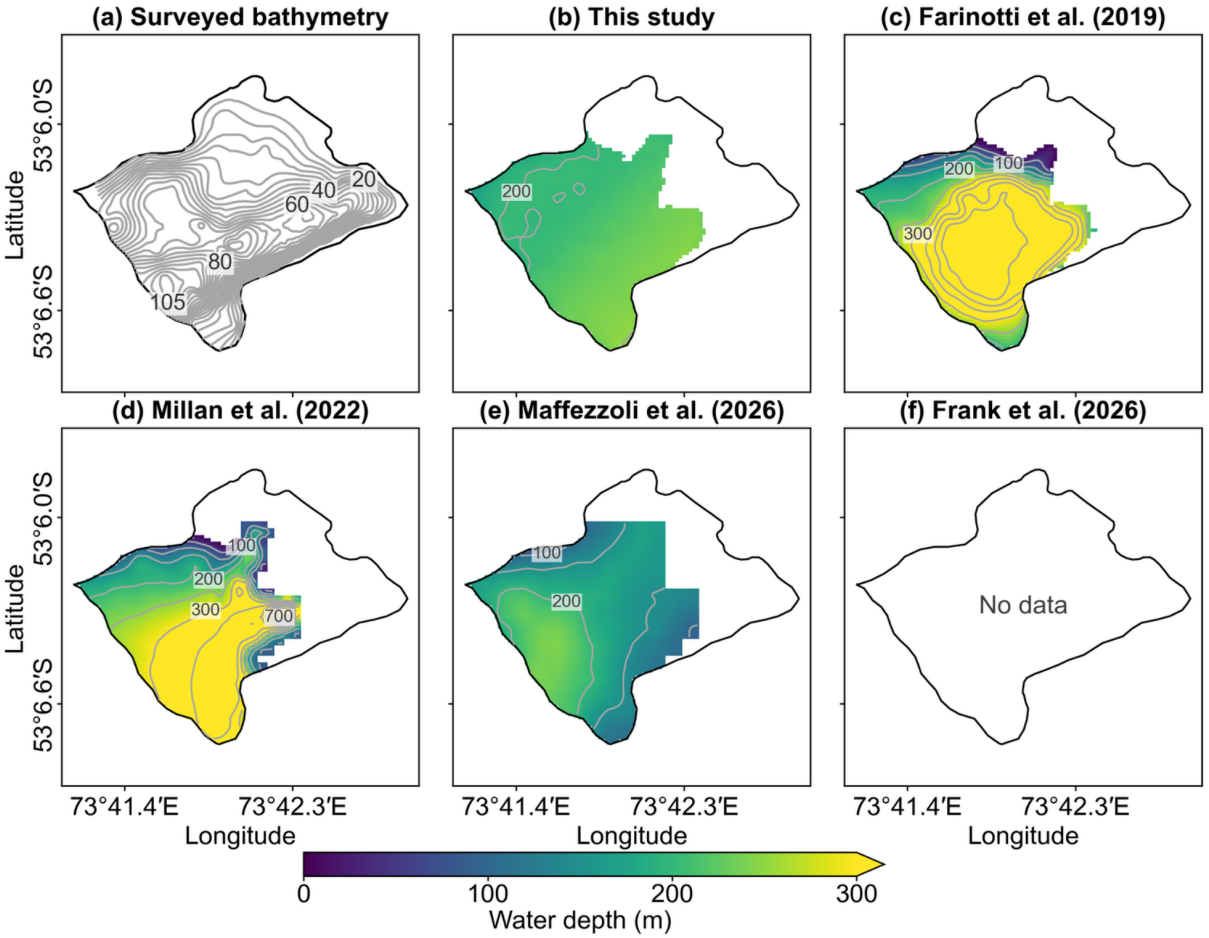

Figure S7. Water depth within the bathymetrically surveyed northern portion of the 2001 Stephenson Lagoon from **(a)** the bathymetric survey (Donoghue, 2009), and **(b-f)** the differences between the glacier surface elevation from 2000 NASADEM and the 1988 ice thickness estimates from **(b)** this study, **(c)** Farinotti et al. (2019), **(d)** Millan et al. (2022), **(e)** Maffezzoli et al. (2026), and **(f)** Frank et al. (2026).

References

Berthier, E., Le Bris, R., Mabileau, L., Testut, L., and Rémy, F.: Ice wastage on the Kerguelen Islands (49° S, 69° E) between 1963 and 2006, J. Geophys. Res.-Earth, 114, F03005, https://doi.org/10.1029/2008JF001192, 2009.

Division of National Mapping: Topographic map of Heard Island. Scale 1: 50 000. MAP G9182.H4. Produced by the Division of National Mapping, Dept. of National Development, https://nla.gov.au/nla.obj-2545184819 (last access: January 2025), 1964.

Donoghue, S. L: Changes in the morphology, mass balance and dynamics of Brown Glacier, Heard Island, with comparisons to the surrounding sub-Antarctic islands, PhD thesis, University of Tasmania, Hobart, Australia, https://doi.org/10.25959/23233313, 2009.

EROS Center: Landsat 7 Enhanced Thematic Mapper Plus Level-2, Collection 2, U.S. Geological Survey [data set], https://doi.org/10.5066/P9C7I13B, 2020.

European Space Agency (ESA): Copernicus DEM – Global and European Digital Elevation Model (COP-DEM), GLO-30, European Space Agency [data set], https://doi.org/10.5270/ESA-c5d3d65, 2021.

Farinotti, D., Huss, M., Fürst, J. J., Landmann, J., Machguth, H., Maussion, F., and Pandit, A.: A consensus estimate for the ice thickness distribution of all glaciers on Earth, Nat. Geosci., 12, 168–173, https://doi.org/10.1038/s41561-019-0300-3, 2019.

Frank, T., van Pelt, W. J. J., Rounce, D. R., Jouvet, G., and Hock, R.: Global glacier-free topography reveals a large potential for future lakes in presently ice-covered terrain, Nat. Commun., 17, 3985, https://doi.org/10.1038/s41467-026-72548-9, 2026.

Frey, H., Machguth, H., Huss, M., Huggel, C., Bajracharya, S., Bolch, T., Kulkarni, A., Linsbauer, A., Salzmann, N., and Stoffel, M.: Estimating the volume of glaciers in the Himalayan–Karakoram region using different methods, The Cryosphere, 8, 2313–2333, https://doi.org/10.5194/tc-8-2313-2014, 2014.

Hugonnet, R., McNabb, R., Berthier, E., Menounos, B., Nuth, C., Girod, L., Farinotti, D., Huss, M., Dussaillant, I., Brun, F., and Kääb, A.: Accelerated global glacier mass loss in the early twenty-first century, Nature, 592, 726–731, https://doi.org/10.1038/s41586-021-03436-z, 2021.

Maffezzoli, N., Rignot, E., Barbante, C., Morlighem, M., Petersen, T. C., and Vascon, S.: Machine-learned global glacier ice volumes, Sci. Data, 13, 1104, https://doi.org/10.1038/s41597-026-07744-9, 2026.

Millan, R., Mouginot, J., Rabatel, A., and Morlighem, M.: Ice velocity and thickness of the world's glaciers, Nat. Geosci., 15, 124–129, https://doi.org/10.1038/s41561-021-00885-z, 2022.

NASA JPL: NASA SRTM-only Height and Height Precision Global 1 arc second V001, NASA Land Processes Distributed Active Archive Center [data set], https://doi.org/10.5067/MEASURES/NASADEM/NASADEM_SHHP.001, (last access: 14 August 2026), 2020.

NASA/METI/AIST/Japan Spacesystems and U.S./Japan ASTER Science Team: ASTER Global Digital Elevation Model V003, NASA Land Processes Distributed Active Archive Center [data set], https://doi.org/10.5067/ASTER/ASTGTM.003, (last access: 14 August 2026), 2019.

RGI Consortium: Randolph Glacier Inventory – A Dataset of Global Glacier Outlines, Version 6.0, NASA National Snow and Ice Data Center Distributed Active Archive Center [data set], https://doi.org/10.7265/4m1f-gd79, (last access: 12 October 2026), 2017.

RGI Consortium: Randolph Glacier Inventory – A Dataset of Global Glacier Outlines, Version 7.0, NASA National Snow and Ice Data Center Distributed Active Archive Center [data set], https://doi.org/10.5067/F6JMOVY5NAVZ, (last access: 12 October 2026), 2023.

Tielidze, L. G., Mackintosh, A. N., and Yang, W.: Glacier inventories reveal an acceleration of Heard Island glacier loss over recent decades, The Cryosphere, 19, 2677–2694, https://doi.org/10.5194/tc-19-2677-2025, 2025.